Ultrasonics Sonochemistry 74 (2021) 105570

Contents lists available at ScienceDirect

Ultrasonics Sonochemistry

journal homepage: www.elsevier.com/locate/ultson

Behaviors and physical mechanism of ceftezole sodium de-agglomeration driven by ultrasound

Xiaowei Cheng [a], Xin Huang [a,b,*], Beiqian Tian [a], Ting Wang [a,b], Hongxun Hao [a,b,c,*]

[a] National Engineering Research Center for Industrial Crystallization Technology, School of Chemical Engineering and Technology, Tianjin University, Tianjin 300072, China
[b] Collaborative Innovation Center of Chemical Science and Engineering (Tianjin), Tianjin 300072, China
[c] School of Chemical Engineering and Technology, Hainan University, Haikou 570208, China

ARTICLE INFO

Keywords:
Ultrasound
Drowning-out crystallization
Ceftezole sodium
De-agglomeration

ABSTRACT

Ultrasound-mediated method, which can effectively disperse agglomerates or even eliminate agglomeration, has received more and more attentions in industrial crystallization. However, the ultrasound-mediated de-agglomeration mechanism has not been well understood, and no general conclusions have been drawn. In this study, the crystallization and de-agglomeration process of ceftezole sodium agglomerates under ultrasound irradiation were systematically investigated. Kapur function was selected to investigate the de-agglomeration process under different ultrasonic powers. The results revealed that ultrasound could efficiently inhibit agglomeration. Besides, the de-agglomeration of large sized agglomerate particles was found to be easier to occur in comparison with small sized particles due to its higher specific breakage rate. Finally, the de-agglomeration mechanism under ultrasonic irradiation was proposed on the basis of the calculated cumulative breakage functions.

1. Introduction

Agglomeration, as a common phenomenon in industrial production, could affect the downstream processing units, end-use properties, as well as the range of applications [1–3]. For example, ceramic agglomerates would depress the shrinkage rate of ceramic powders during sintering and further hamper densification of ceramic parts [4]. For paints, agglomerates of the pigmentary particles would degrade the uniformity of paint [5]. For active pharmaceutical ingredients, irregular agglomerates can decline the efficiency of filtration, washing, drying, and reduce the purity of the product as mother liquor and impurities would entrap into the agglomerates [6]. Thus, further unit operations need to be adopted to ensure the high quality of the final products in industrial manufacture, which is undesirable in industry due to higher time and cost consuming. Therefore, it is of great importance to eliminate agglomeration and reduce the negative effects as much as possible in the crystallization process.

Ultrasound-mediated method, which can effectively disperse agglomerates or even eliminate agglomeration without the introduction of additives, has received more and more attentions recently [7–13]. It has been confirmed that the dispersion efficiency of agglomerate particles under ultrasonic irradiation is much larger than that of mechanical stirring at lower input power [14]. Besides, many researches have shown that particles obtained under ultrasonic irradiation can not only have a favorable dispersion, but also show desirable physicochemical properties. Mahbubul's group investigated the effect of ultrasonication on the dispersion and stability of nanofluids with direct sonication. The results showed that ultrasonication had a positive impact on dispersion properties of TiO_2 – water nanofluid. Moreover, the obtained nanofluid under 150 min of ultrasonication yielded the highest stability [15]. Mendoza's group performed a series of experiments focused on the effects of irradiated volume, sonication time, as well as sonication power on the de-agglomeration of NaX zeolites. The investigating results demonstrated that the agglomerates population was reduced after ultrasonic irradiation, while the tapped density of NaX zeolites was improved in comparison with the absence of ultrasonication [16]. Shahcheraghi's group showed that nano-copper oxides with certain particle size could be rapidly produced in an ultrasonic system, and the nanoparticles had high purity [17].

Besides, some researches explored the de-agglomeration mechanism of ultrasonic irradiation. Kumar's group reported that the predominant mechanism for the breakup of agglomeration of hydrophilic famed silica

* Corresponding authors at: National Engineering Research Center for Industrial Crystallization Technology, School of Chemical Engineering and Technology, Tianjin University, Tianjin 300072, China (X. Huang); School of Chemical Engineering and Technology, Hainan University, Haikou 570208, China (H. Hao).
E-mail addresses: x_huang@tju.edu.cn (X. Huang), hongxunhao@tju.edu.cn (H. Hao).

https://doi.org/10.1016/j.ultsonch.2021.105570
Received 3 February 2021; Received in revised form 6 April 2021; Accepted 16 April 2021
Available online 20 April 2021

nanoparticles was erosion based on the scattering light characterization [18]. Sauter's group put forward that ultrasound mediated de-agglomeration of SiO_2 particles was considered to be mainly a result of cavitation [19]. Jone's group suggested that agglomeration was inhibited as the cavitation bubbles collapse to break the interaction between fine crystals and agglomerates [20]. Gerven's group suggested that ultrasound introduction enhanced suspension micromixing, which increased interparticles collisions frequency, leading to preventing forming agglomerates [21], while Suslick's group found that high velocity interparticles collisions could lead to extreme heating at the point of impact, which could result in local melting and further formed agglomerates [22,23]. Thus, the mechanism of de-agglomeration under ultrasonic irradiation has still not been well understood and no general rules or theories have been established. More systematic researches need to be conducted to further unveil the ultrasound-mediated de-agglomeration mechanism, especially for the organic compounds (active pharmaceutical ingredient et al.), which are rarely studied compared to inorganic compounds.

Hence, in this study, ceftezole sodium, a first-generation cephalosporin antibiotic, was selected as the model compound to investigate the de-agglomeration process and explore the de-agglomeration mechanism. Firstly, sonocrystallization process of ceftezole sodium was investigated under different ultrasonic powers and sonication time. Subsequently, the ultrasound-mediated de-agglomeration was explored at various ultrasonic powers on the basis of the Kapur function. Finally, the de-agglomeration mechanism was proposed depending on the calculated cumulative breakage distribution functions.

2. Theories

Breakage function and selection function are used in the Kapur functions to characterize the breakage. The selection function (S_i) is the breakage rate constant of particles size x_i. The cumulative breakage function ($B_{i,j}$) gives the distribution of fragments from breakage of size x_j to have a size less than x_i [24,25]. The cumulative oversize fraction used during Kapur function analysis for batch breakage can be written as the following equation [25,26]

$$R(x,t) = R(x,0)exp\left[\sum_{k=1}^{P} K^{(k)}(x)\frac{t^k}{k!}\right] \quad (1)$$

where $R(x,t)$ is the cumulative oversize fraction above particle size x at any instant of time t. $R(x,0)$ is the corresponding cumulative oversize fraction at the beginning of breakage. The terms in the bracket are known as the Kapur function from which the approximate specific breakage rate (S_i) and cumulative breakage function ($B_{i,j}$) can be derived. At any time t, a residual ratio can be defined as:

$$f(x,t) = \frac{R(x,t)}{R(x,0)} \quad (2)$$

For short breakage time, Eq. (1) can be simplified to the following equation

$$f(x,t) = exp\left(K^{(1)}t\right) \quad (3)$$

The first Kapur function $K^{(1)}$ can be obtained by plotting ln $f(x,t)$ against time. Then, the specific breakage rate and cumulative breakage function at different particle size classes can be calculated as the following equations.

$$S_i = -K_i^{(1)} \quad (4)$$

$$B_{i,j} = \frac{K_i^{(1)}}{K_j^{(1)}} \quad (5)$$

The available breakage time for estimating the breakage parameters using Eq. (3) may be different for different systems, as the different properties of the materials and the efficiency of the equipment. The available breakage time, which could define Eq. (3) could be used or not for estimating the breakage parameters, can be determined by the following equation

$$T = 100\left[1 - e^{-S_1 t}\right] \quad (6)$$

where S_1 is the breakage rate constant of particle class 1, t is the actual breakage time. T is the dimensionless time. If T is above 95%, Eq. (3) is not recommended for estimating the parameters [27].

Numbering of the particle size classes is done in reverse order. Namely, the coarsest size class is named as 1, and the class numbering ascends toward the finest size. Then, the curve B_{ij} against x_i/x_j can be used to determine the breakage mechanism: fracture and abrasion. Fracture mechanism is defined as original particles are split into variably sized smaller particles. In contrast, abrasion is the mechanism by which smaller particles are chipped away from the edges and surfaces of the original particles [24,25,28]. If the curve is nearer to the extreme fracture curve, the breakage mechanism would be dominantly controlled by fracture and vice versa.

3. Experimental

3.1. Materials

Ceftezole sodium (99%) was provided by Shandong Lukang Pharmaceutical Co., Ltd., China. Anhydrous ethanol with analytical reagent grade was purchased from Tianjin Yuxiang Chemical Reagent Co., Ltd., China. Deionized water was prepared by the Millipore water system with a resistivity of 18.2 MΩ·cm at 298.15 K. All of the chemicals were used without further purification.

3.2. Sonocrystallization experiments

25 mL of 11% (w/v) ceftezole sodium aqueous solution was prepared and filtered into a 120 mL jacketed crystallizer by 0.22 μm syringe filter. Then 80 mL anhydrous ethanol was pumped into the solution at a speed of 2 mL/min by a peristaltic pump (BT100-1F, LongerPump, China). At the same time, two kinds of ultrasonic irradiation were applied into the working solution until the end of the poor solvent addition: continuous and intermittent ultrasonic irradiation. For continuous ultrasonic irradiation, a series of ultrasonic powers (80–320 W) were applied into the solution all the time. For intermittent ultrasonic irradiation, a fixed power of 80 W was applied with sonication of 1 min duration after the addition of every 6 mL, 14 mL, 38 mL anhydrous ethanol. Thus, the total sonication time corresponded to 10 min, 5 min, 2 min, respectively. For the comparison, the crystallization without ultrasound introduction was also conducted at the similar condition of ultrasound introduction. A summary of the experimental conditions was summarized as category 1 in Table 1. At the end of the experiments, 2 mL suspensions were taken out to analyze the crystal size distribution with the dispersed phase of cold anhydrous ethanol which was beforehand stored in the jacketed crystallizer using a Malvern Mastersizer 3000 (Malvern Instruments Ltd.). The jacketed crystallizer and the experimental temperature was kept at 283.15 K controlled by thermostatic water bath (CF41, Julabo, Germany) and the stirring speed of 250 rpm was controlled by magnetic stirrer (ZNCL-BS, Xingke Sci. Ltd., China). During all the experiments, ultrasonic irradiation frequency was fixed at 20 kHZ using an ultrasonic processor (UP-400S, Jingxin, China) with the tip diameter of 5 mm providing a maximum irradiation power of 400 W.

3.3. Particle de-agglomeration experiments

Ceftezole sodium particles with the mean particle size around 55.5 μm (2.0000 ± 0.0010 g) was suspended into 210 mL anhydrous ethanol–water mixed solvents ($V_{ethanol}$:V_{water} = 3.2) at 283.15 K and stirring

Table 1
The experimental parameters used in sonocrystallization and de-agglomeration experiments.

Conditions		Sonocrystallization experiments category 1		Conditions	De-agglomeration experiments category 2	
		Ultrasonic power	Sonication time		Ultrasonic power	Sonication time
Continuous ultrasound	1	80 W	40 min	1	80 W	30 min
	2	160 W	40 min	2	160 W	30 min
	3	240 W	40 min	3	240 W	30 min
	4	320 W	40 min	4	320 W	30 min
Intermittent ultrasound	5	80 W	0 min			
	6	80 W	2 min			
	7	80 W	5 min			
	8	80 W	10 min			

speed of 250 rpm. Then continuous ultrasonic irradiations of 80–320 W with 80 W interval power were introduced to the suspension, and which was lasted for 30 min. The experimental conditions were summarized as category 2 in Table 1. Then 2 mL suspension samples were taken at the beginning of the de-agglomeration experiments and with a constant time interval after the ultrasonic introduction. These suspension samples were dispersed into the cold anhydrous ethanol which was beforehand stored in the jacketed crystallizer for analyzing particle size distribution with a Malvern Mastersizer 3000 (Malvern Instruments Ltd.). The temperature of the jacketed crystallizer was maintained at 283.15 K by the thermostatic water bath (CF41, Julabo, Germany).

4. Results and discussions

4.1. Sonorystallization experiments

The effects of the ultrasonic power and sonication time on the sonocrystallization of ceftezole sodium were investigated systematically. In this work, the increase of ceftezole sodium particles size is mainly ascribed to the spherical agglomeration of ceftezole sodium particles, which is a fast process, as shown in Fig. 1. Therefore, the change of particles size is related to agglomeration process. The contour plots of the particle size distributions under different ultrasonic powers and sonication times are shown in Fig. 2. It could be seen from Fig. 2(a) that the mean particle size decreases with the increasing of sonication time under the ultrasound introduction, whose detailed data are shown in Table S1 in the Supporting information. Moreover, the width of particle size distributions in the contour plot under ultrasound is larger than that without ultrasound. The coefficient of variation (CV) could characterize the particle size distribution. It could be calculated by $CV = (PD_{84\%} - PD_{16\%})/2PD_{50\%}$. The smaller the CV value is, the more uniform the particle size will be. It could be found that CV value becomes larger with the ultrasound application (Table S1). It means poorer uniformity of particle size of the product. Moreover, from Fig. 3(b, c), both smaller agglomerates and single crystals could be observed. The CV value gets smaller under the sonication time of 10 min, indicating the presence of more uniform particles. From Fig. 3d, little agglomeration exists after 10 min of sonication time. All the results indicate that less agglomerates existed and more fine single crystals existed with the increasing of sonication time. Similarly, the mean particle sizes under different ultrasonic powers decrease to be almost 10 μm, as shown in Fig. 2(b). Furthermore, the mean particle size declines with the

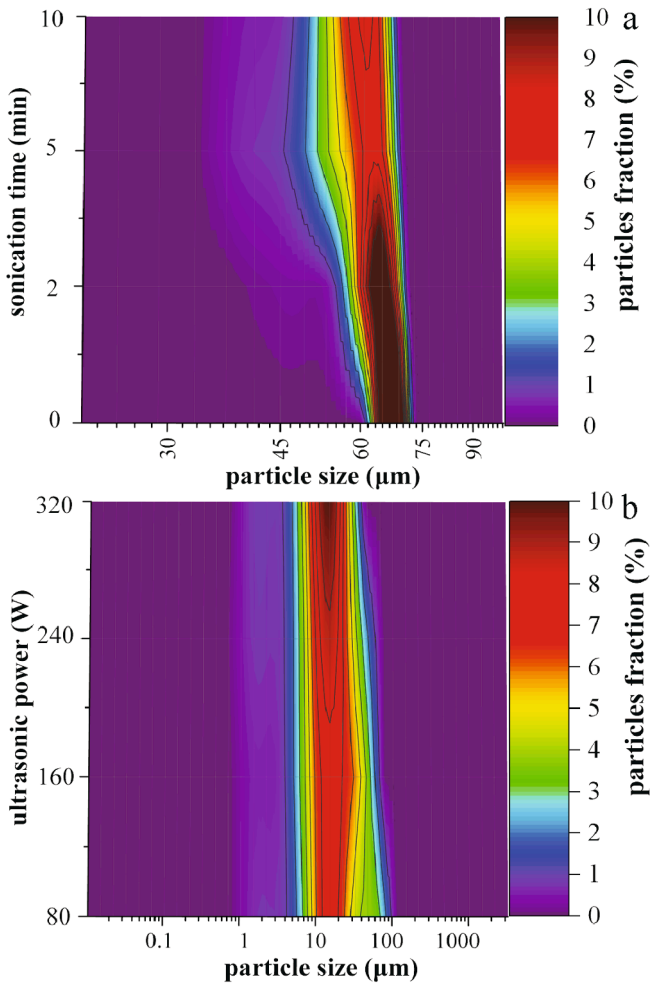

Fig. 2. The contour plots of particle size distributions under different sonication times at the fixed ultrasonic power of 80 W (a) and different ultrasonic powers at the fixed sonication time of 40 min (b).

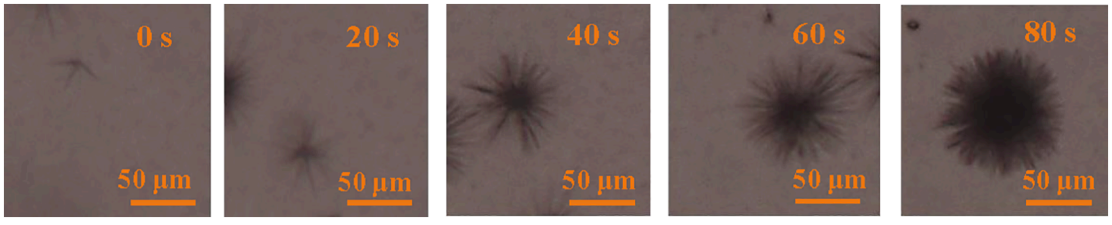

Fig. 1. The microscopic photos showing the spherical agglomeration process of ceftezole sodium.

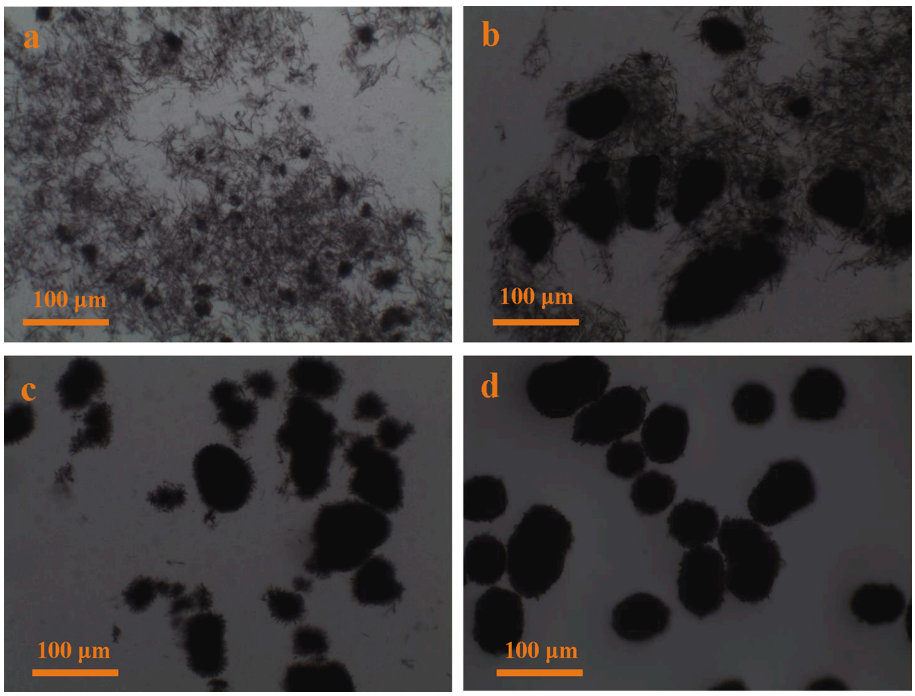

Fig. 3. Microscope images for ceftezole sodium crystals obtained at different sonication time and fixed ultrasonic power of 80 W. a) intermittent ultrasonic irradiation at 10 min. b) intermittent ultrasonic irradiation at 5 min. c) intermittent ultrasonic irradiation at 2 min. d) without ultrasonic irradiation.

ultrasonic power increasing (see Table S1). In addition, the widths of the particle size distribution also decline with the increasing of ultrasonic power (Fig. 2(b), Table S1). It means the particle size distribution of the products tends to be more uniform. It could also be found from Fig. 4 that the obtained products are almost fine dispersed crystals. All the results indicate that products with more fine dispersed crystals would be obtained under higher ultrasonic power.

Therefore, it could be concluded that agglomeration could be inhibited with the application of ultrasound. The reasons may be that the cavitation bubbles prefer to attach to the agglomerates surface due to the large particle size and the collapse of bubbles would cause shock wave to break the interaction between the agglomerates and the fine

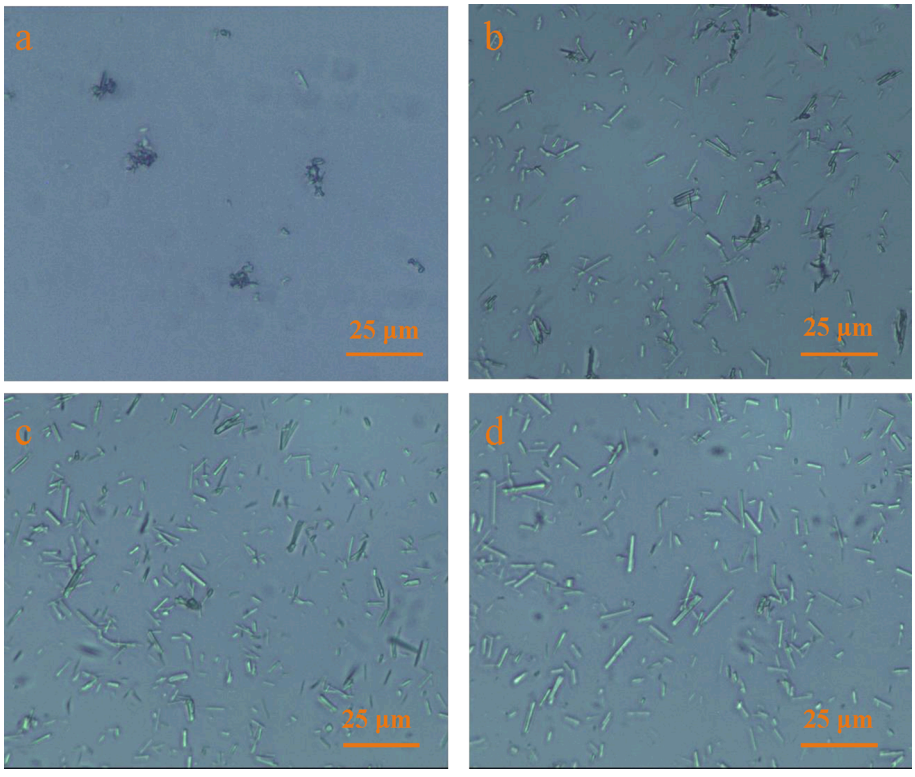

Fig. 4. Microscope images for ceftezole sodium crystals obtained at fixed 40 min of sonication time and different ultrasonic powers. a) continuous ultrasonic irradiation at 80 W. b) continuous ultrasonic irradiation at 160 W. c) continuous ultrasonic irradiation at 240 W. d) continuous ultrasonic irradiation at 320 W.

particles, and thus discrete and fine dispersed particles reattachments will be prevented [20]. As the ultrasonic power and sonication time raise, the cavitation is intensified [29]. More cavitation bubbles attached onto the agglomerates surface would also enhance the breakage of agglomerates. Therefore, de-agglomeration will be more efficient under higher ultrasound power and longer sonication time.

4.2. Kinetic modeling of de-agglomeration

In order to further determine the de-agglomeration mechanism at ultrasonic irradiation, cumulative breakage functions under different conditions were investigated. Firstly, it is confirmed that stirring speed of 250 rpm in this study has a negligible effect on the particle de-agglomeration as tested by the mean particle size under stirring over 60 min without ultrasound, as shown in Fig. 5. The mean particle size is 55.5 μm at the beginning and 55.0 μm after 60 min stirring. Therefore, the effect of stirring at 250 rpm on particle size can be ignored and the ultrasound should be the main factor to cause the particles de-agglomeration.

As shown in Section 2, T is used to determine whether Eq. (3) could be used or not for estimating the breakage parameters. Considering T should not be above 95, Eq. (3) could be used for estimating the breakage parameters. In this study, t is selected as 12 min for further analysis, so that the T in all cases is below 95. Subsequently, the kinetic modeling via Kapur function was carried out to determine the breakage rate of the particles. Firstly, 10 particle size classes were classified for particle size ranging between 4.03 and 76.01 μm, as shown in Table 2. Then, the residual ratios $f(x,t)$ could be obtained for each particle class by Eq. (2). Then, the first Kapur functions were obtained from the slopes of the plotting of ln ($f(x,t)$) versus time and the results are shown in Fig. S1. Then, the specific breakage rate, S_i, can be determined by the Eq. (4). The obtained results are listed in Table S2, which shows good fitting results with R^2 exceeding 0.95. Special breakage rates of particle class 1 under 80 W, 160 W, 240 W, and 320 W ultrasonic powers are 1.29×10^{-3} s^{-1}, 1.74×10^{-3} s^{-1}, 2.09×10^{-3} s^{-1}, and 4.10×10^{-3} s^{-1}, respectively, while particle class 10 show lower breakage rates, namely, 6.05×10^{-6}, 6.42×10^{-6}, 6.52×10^{-6}, and 7.05×10^{-6} s^{-1} under the corresponding conditions (Table S2). The specific breakage rate of particle class 1 under 320 W ultrasonic power is almost three times larger than that under 80 W ultrasonic power. However, specific breakage rate of particle class 10 under 320 W ultrasonic power is almost one time larger than that under 80 W ultrasonic power.

To show clearly the effect of ultrasonic power on specific breakage rates of different particle size products, the specific breakage rates of the products with different particle size classes under different ultrasonic powers are shown in Fig. 6. As shown in Fig. 6, the specific breakage rate of all particle size classes increases as the ultrasonic power increases. The specific breakage rates of products with large particle size increases dramatically than those of small particle sized products with ultrasonic power increasing. It indicates that products with larger particles size not only possess larger specific breakage rates, but also are more strongly affected by ultrasonic power. Therefore, it could draw a conclusion that the de-agglomeration is much easier to occur under higher ultrasonic power, and de-agglomeration of large sized agglomerate particles is more remarkable than that of small sized particles. Based on the specific breakage rates, the cumulative breakage functions $B_{i,j}$ for different ultrasonic powers were calculated by Eq. (5). $B_{i,j}$ for various particle size classes under different ultrasonic powers are shown in Fig. 7. It could be seen from Fig. 7 that $B_{i,j}$ generally lies around the extreme curve of fracture. Moreover, B_{ij} is nearer to the fracture curve under the higher ultrasonic power, such as 320 W. It means that the de-agglomeration mechanism under ultrasound of particles is dominated mainly by fracture.

Table 2
Definition of particle size classes.

Particle classes i,j	Particle size range, μm
1	>76.01
2	66.90–76.01
3	58.88–66.90
4	51.82–58.88
5	45.61–51.82
6	31.10–45.61
7	21.21–31.10
8	14.46–21.21
9	8.68–14.46
10	4.03–8.68

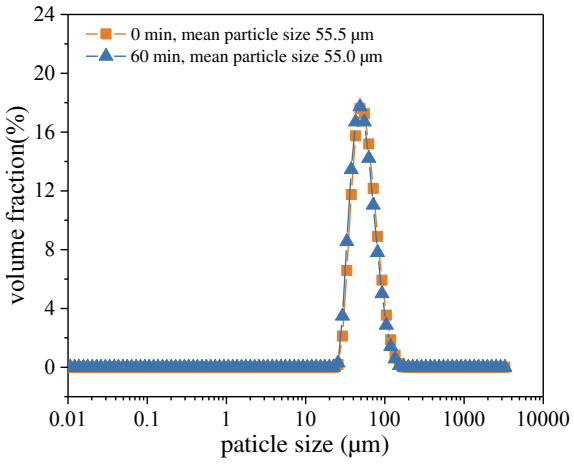

Fig. 5. The particle size distributions of ceftezole sodium products agitated for 0 min and 60 min under no ultrasound.

4.3. De-agglomeration mechanism

By the above analysis, a proposed de-agglomeration mechanism is given to understand the de-agglomeration process as shown in Fig. 8. When the ultrasound is introduced into the solution, the cavitation phenomena which is the formation, growth, and collapse of bubbles is created by the pressure variation [30–32]. Cavitation bubbles may

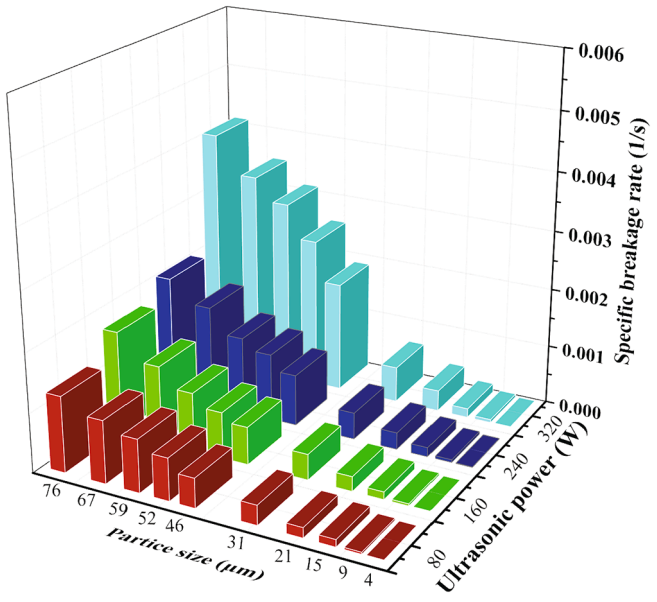

Fig. 6. The specific breakage rates of products with different particle size at different ultrasonic powers. The particle sizes used in this figure corresponded to the minimum particle size of each particle size class.

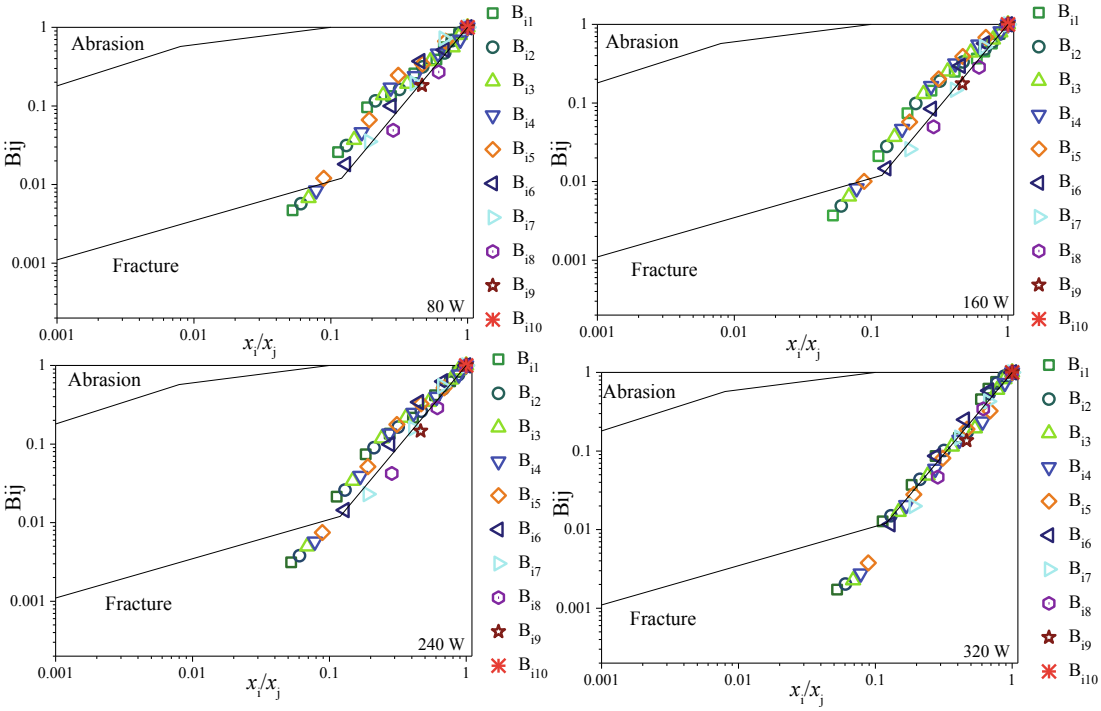

Fig. 7. Cumulative breakage functions B_{ij} for all particle size classes at different ultrasonic powers. The B_{ij} for abrasion and fracture curves obtained from the literatures [24,25].

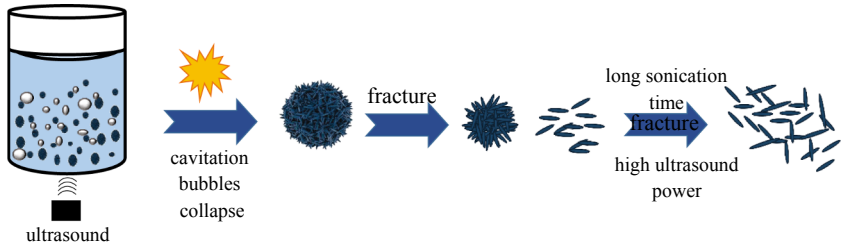

Fig. 8. Schematic representation of the proposed de-agglomeration mechanism under ultrasound.

prefer to attach to the agglomerates with the large particle size and have a high significance on the agglomerates. During the compression and rarefaction of phases, cavitation bubbles attached onto the agglomerates collapse and release shock waves. The released shock waves might break the agglomerates mainly by fracture, namely, splitting the agglomerates into smaller sized particles. Therefore, the agglomeration is inhibited during the sonocrystallization process.

5. Conclusions

In this study, the behaviors and de-agglomeration mechanism of ceftezole sodium were investigated under ultrasound irradiation. Particle size distribution and Kapur function were selected to investigate agglomeration of ceftezole sodium agglomerates under ultrasonic irradiation. All the results indicated that the application of the ultrasound could efficiently inhibit agglomeration. Moreover, de-agglomeration of large sized agglomerate particles was more facilitated to occur in comparison with small sized particles due to the higher breakage rate, which was positive relevant to ultrasonic power. Depended on the calculated cumulative breakage functions, the de-agglomeration mechanism under ultrasonic irradiation was proposed as cavitation bubbles attached onto the agglomerates collapsed and released shock wave to split the agglomerates into smaller sized particles mainly by fracture.

CRediT authorship contribution statement

Xiaowei Cheng: Methodology, Formal analysis, Investigation, Writing - original draft. **Xin Huang:** Writing - review & editing, Funding acquisition. **Beiqian Tian:** Resources. **Ting Wang:** Resources. **Hongxun Hao:** Writing - review & editing, Funding acquisition, Supervision.

Declaration of Competing Interest

The authors declare that they have no known competing financial interests or personal relationships that could have appeared to influence the work reported in this paper.

Acknowledgements

This research is financially supported by National Natural Science Foundation of China (No. 21908159) and China Postdoctoral Science Foundation (No. 2019M651039).

Appendix A. Supplementary data

Supplementary data to this article can be found online at https://doi.org/10.1016/j.ultsonch.2021.105570.

References

[1] Y.A. Abramov, Understanding the risk of agglomeration of polar pharmaceutical crystals, Cryst. Growth Des. 17 (2017) 2873–2880, https://doi.org/10.1021/acs.cgd.7b00429.

[2] W. Yang, L. Zhou, J. Dai, L. Zhou, M. Zhang, C. Xie, H. Hao, B. Hou, Y. Bao, Q. Yin, Crystallization of lithium carbonate from aqueous solution: new insights into crystal agglomeration, Ind. Eng. Chem. Res. 58 (2019) 18448–18455, https://doi.org/10.1021/acs.iecr.9b03644.

[3] X. Cheng, F. Li, L. Luo, Z. Ding, L. Zeng, Y. Mao, X. Huang, H. Hao, On the selection of wetting liquid for spherical agglomeration of cefotaxime sodium, Powder Technol. 363 (2020) 593–601, https://doi.org/10.1016/j.powtec.2019.12.002.

[4] F.W. Dynys, J.W. Halloran, Influence of aggregates on sintering, J. Am. Ceram. Soc. 67 (1984) 596–601, https://doi.org/10.1111/j.1151-2916.1984.tb19601.x.

[5] K.A. Kusters, S.E. Pratsinis, S.G. Thoma, D.M. Smith, Ultrasonic fragmentation of agglomerate powders, Chem. Eng. Sci. 48 (1993) 4119–4127, https://doi.org/10.1016/0009-2509(93)80258-r.

[6] X. Cheng, X. Zhang, X. Huang, T. Wang, H. Hao, Insight into the growth of ordered agglomerates based on oriented attachment, J. Mol. Liq. (2020), https://doi.org/10.1016/j.molliq.2020.114844. Ahead of Print.

[7] M. Ashokkumar, J. Lee, S. Kentish, F. Grieser, Bubbles in an acoustic field: an overview, Ultrason. Sonochem. 14 (2007) 470–475, https://doi.org/10.1016/j.ultsonch.2006.09.016.

[8] R.M. Wagterveld, L. Boels, M.J. Mayer, G.J. Witkamp, Visualization of acoustic cavitation effects on suspended calcite crystals, Ultrason. Sonochem. 18 (2010) 216–225, https://doi.org/10.1016/j.ultsonch.2010.05.006.

[9] Y. Mao, F. Li, T. Wang, X. Cheng, G. Li, D. Li, X. Zhang, H. Hao, Enhancement of lysozyme crystallization under ultrasound field, Ultrason. Sonochem. 63 (2020), https://doi.org/10.1016/j.ultsonch.2020.104975.

[10] S. Markovic, M. Mitric, G. Starcevic, D. Uskokovic, Ultrasonic de-agglomeration of barium titanate powder, Ultrason. Sonochem. 15 (2008) 16–20, https://doi.org/10.1016/j.ultsonch.2007.07.008.

[11] S. Nalesso, M.J. Bussemaker, R.P. Sear, M. Hodnett, J. Lee, A review on possible mechanisms of sonocrystallisation in solution, Ultrason. Sonochem. 57 (2019) 125–138, https://doi.org/10.1016/j.ultsonch.2019.04.020.

[12] V.S. Nguyen, D. Rouxel, R. Hadji, B. Vincent, Y. Fort, Effect of ultrasonication and dispersion stability on the cluster size of alumina nanoscale particles in aqueous solutions, Ultrason. Sonochem. 18 (2010) 382–388, https://doi.org/10.1016/j.ultsonch.2010.07.003.

[13] B.W. Zeiger, K.S. Suslick, Sonofragmentation of molecular crystals, J. Am. Chem. Soc. 133 (2011) 14530–14533, https://doi.org/10.1021/ja205867f.

[14] S. Sumitomo, H. Koizumi, M.A. Uddin, Y. Kato, Comparison of dispersion behavior of agglomerated particles in liquid between ultrasonic irradiation and mechanical stirring, Ultrason. Sonochem. 40 (2018) 822–831, https://doi.org/10.1016/j.ultsonch.2017.08.023.

[15] I.M. Mahbubul, E.B. Elcioglu, R. Saidur, M.A. Amalina, Optimization of ultrasonication period for better dispersion and stability of TiO_2-water nanofluid, Ultrason. Sonochem. 37 (2017) 360–367, https://doi.org/10.1016/j.ultsonch.2017.01.024.

[16] H. Ramirez Mendoza, J. Jordens, M. Valdez Lancinha Pereira, C. Lutz, T. Van Gerven, Effects of ultrasonic irradiation on crystallization kinetics, morphological and structural properties of zeolite FAU, Ultrason. Sonochem. 64 (2020), https://doi.org/10.1016/j.ultsonch.2020.105010fav.

[17] S.H. Shahcheraghi, M. Schaffie, M. Ranjbar, Development of an electrochemical process for production of nano-copper oxides: agglomeration kinetics modeling, Ultrason. Sonochem. 44 (2018) 162–170, https://doi.org/10.1016/j.ultsonch.2018.02.024.

[18] Vikash, V. Kumar, Ultrasonic-assisted de-agglomeration and power draw characterization of silica nanoparticles, Ultrason. Sonochem. 65 (2020), https://doi.org/10.1016/j.ultsonch.2020.105061.

[19] C. Sauter, M.A. Emin, H.P. Schuchmann, S. Tavman, Influence of hydrostatic pressure and sound amplitude on the ultrasound induced dispersion and de-agglomeration of nanoparticles, Ultrason. Sonochem. 15 (2008) 517–523, https://doi.org/10.1016/j.ultsonch.2007.08.010.

[20] Z. Guo, A.G. Jones, N. Li, S. Germana, High-speed observation of the effects of ultrasound on liquid mixing and agglomerated crystal breakage processes, Powder Technol. 171 (2007) 146–153, https://doi.org/10.1016/j.powtec.2006.10.026.

[21] B. Gielen, J. Jordens, L.C.J. Thomassen, L. Braeken, T. Van Gerven, Agglomeration control during ultrasonic crystallization of an active pharmaceutical ingredient, Crystals 7 (2017), https://doi.org/10.3390/cryst7020040, 40/41–40/20.

[22] T. Prozorov, R. Prozorov, K.S. Suslick, High-velocity interparticle collisions driven by ultrasound, J. Am. Chem. Soc. 126 (2004) 13890–13891, https://doi.org/10.1021/ja049493o.

[23] S.J. Doktycz, K.S. Suslick, Interparticle collisions driven by ultrasound, Science 247 (1990) 1067–1069, https://doi.org/10.1126/science.2309118.

[24] J. Jordens, T. Appermont, B. Gielen, T. Van Gerven, L. Braeken, Sonofragmentation: effect of ultrasound frequency and power on particle breakage, Cryst. Growth Des. 16 (2016) 6167–6177, https://doi.org/10.1021/acs.cgd.6b00088.

[25] V. Raman, A. Abbas, W. Zhu, Particle grinding by high-intensity ultrasound: kinetic modeling and identification of breakage mechanisms, AIChE J. 57 (2011) 2025–2035, https://doi.org/10.1002/aic.12415.

[26] H. Berthiaux, C. Varinot, J. Dodds, Approximate calculation of breakage parameters from batch grinding tests, Chem. Eng. Sci. 51 (1996) 4509–4516, https://doi.org/10.1016/0009-2509(96)00275-8.

[27] P.C. Kapur, An improved method for estimating the feed-size breakage distribution functions, Powder Technol. 33 (1982) 269–275, https://doi.org/10.1016/0032-5910(82)85066-3.

[28] J.M. Menacho, Some solutions for the kinetics of combined fracture and abrasion breakage, Powder Technol. 49 (1986) 87–95, https://doi.org/10.1016/0032-5910(86)85010-0.

[29] P.R. Gogate, S. Shaha, L. Csoka, Intensification of cavitational activity in the sonochemical reactors using gaseous additives, Chem. Eng. J. 239 (2014) 364–372, https://doi.org/10.1016/j.cej.2013.11.004.

[30] A.H. Batghare, K. Roy, V.S. Moholkar, Investigations in physical mechanism of ultrasound-assisted antisolvent batch crystallization of lactose monohydrate from aqueous solutions, Ultrason. Sonochem. 67 (2020), https://doi.org/10.1016/j.ultsonch.2020.105127.

[31] C. Cogne, S. Labouret, R. Peczalski, O. Louisnard, F. Baillon, F. Espitalier, Theoretical model of ice nucleation induced by acoustic cavitation. Part 1: Pressure and temperature profiles around a single bubble, Ultrason. Sonochem. 29 (2016) 447–454, https://doi.org/10.1016/j.ultsonch.2015.05.038.

[32] M.D. Luque de Castro, F. Priego-Capote, Ultrasound-assisted crystallization (sonocrystallization), Ultrason. Sonochem. 14 (2007) 717–724, https://doi.org/10.1016/j.ultsonch.2006.12.004.